Volume 5
Number 8
21 April 2023
Pages 2123–2362

Nanoscale Advances

rsc.li/nanoscale-advances

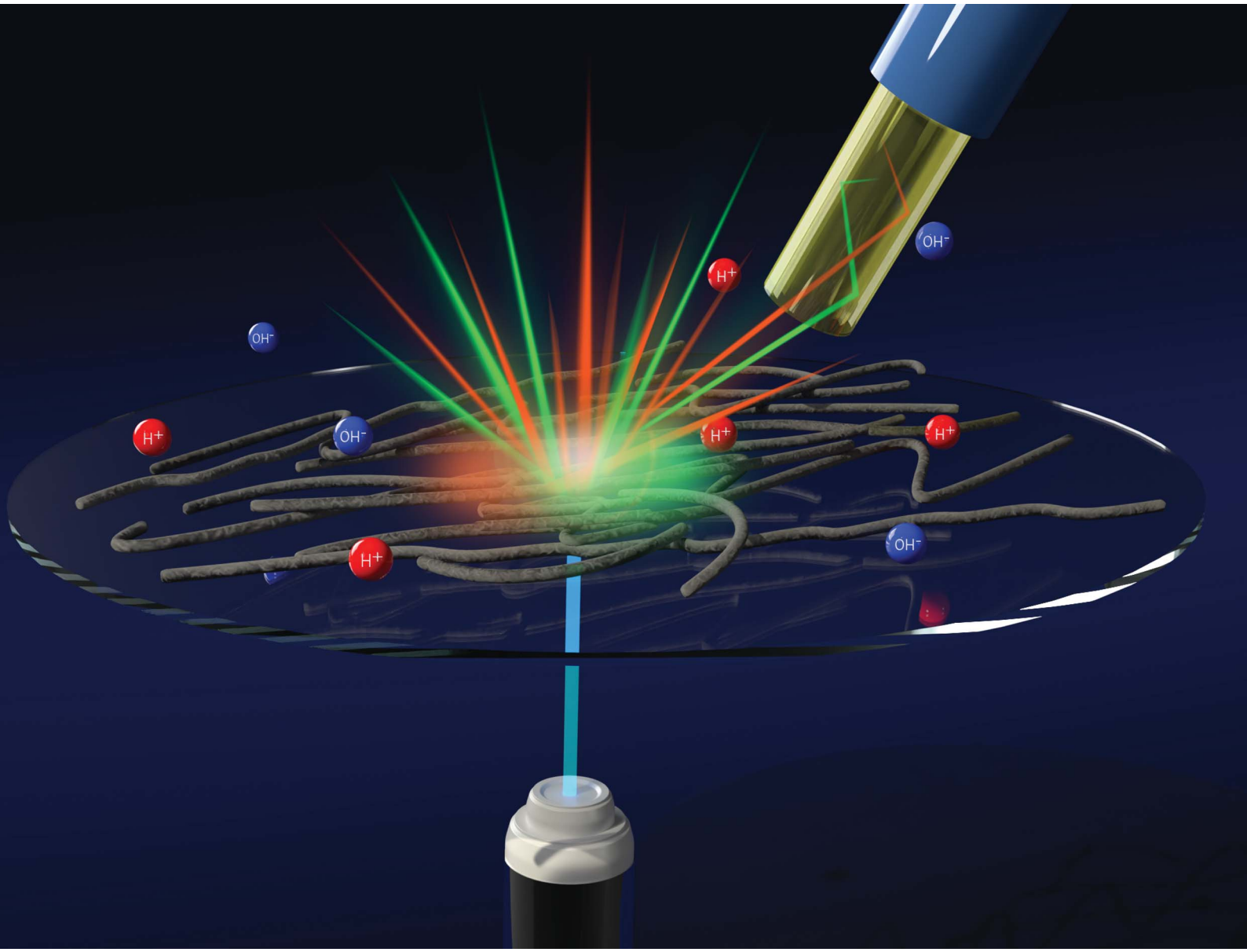

ISSN 2516-0230

ROYAL SOCIETY OF CHEMISTRY

PAPER
John X. J. Zhang *et al.*
Dual fluorescent hollow silica nanofibers for *in situ* pH monitoring using an optical fiber

NCNST

Nanoscale Advances

ROYAL SOCIETY OF CHEMISTRY

PAPER

View Article Online
View Journal | View Issue

Cite this: *Nanoscale Adv.*, 2023, **5**, 2180

Dual fluorescent hollow silica nanofibers for *in situ* pH monitoring using an optical fiber†

Junhu Zhou, ‡ Yundong Ren,‡ Yuan Nie, Congran Jin, Jiyoon Park and John X. J. Zhang*

This study reports a sensitive and robust pH sensor based on dual fluorescent doped hollow silica nanofibers (hSNFs) for *in situ* and real-time pH monitoring. Fluorescein isothiocyanate (FITC) and tris(2,2′-bipyridyl) dichlororuthenium(II) hexahydrate ($Ru(BPY)_3$) were chosen as a pH sensitive dye and reference dye, respectively. hSNFs were synthesized using a two-step method in a reverse micelle system and were shown to have an average length of 6.20 μm and average diameter of 410 nm. The peak intensity ratio of FITC/$Ru(BPY)_3$ was used to calibrate to solution pH changes. An optical-fiber-based fluorescence detection system was developed that enabled feasible and highly efficient near-field fluorescence detection. The developed system enables fully automated fluorescence detection, where components including the light source, detector, and data acquisition unit are all controlled by a computer. The results show that the developed pH sensor works in a linear range of pH 4.0–9.0 with a fast response time of less than 10 s and minimal sample volume of 50 μL, and can be stored under dark conditions for one month without failure. In addition, the as-prepared hSNF-based pH sensors also have excellent long-term durability. Experimental results from ratiometric sensing confirm the high feasibility, accuracy, stability and simplicity of the dual fluorescent hSNF sensors for the detection of pH in real samples.

Received 23rd December 2022
Accepted 15th January 2023

DOI: 10.1039/d2na00943a

rsc.li/nanoscale-advances

1 Introduction

Real-time pH measurements are of great importance in chemical reactions,[1] environmental monitoring,[2] and physiological processes.[3,4] Measuring pH values, especially in small volumes, is difficult but necessary for a variety of scientific applications. For instance, it is well known that the local microenvironment pH has a great influence on immunization, cell metabolism, and enzyme activity.[5–7] Commercially available glass electrode pH sensors are widely used in laboratories for pH measurements. However, the glass electrode pH sensors have disadvantages such as limited accessibility for low volume detection, slow drift, and being unsuitable for long-term pH monitoring.[8,9] Furthermore, glass-electrode-based pH probes have an inherent measurement error on the order of 0.1 pH unit, which limits their use in precision measurements.[10] Optical pH sensors have been proved to be an ideal alternative because of their advantages including rapid response, low sample volume, and the possibility of contactless measurement.[11,12]

Many optical transducers such as organic molecules have been widely used to monitor local pH values. These organic molecules' fluorescence intensity changes when the environmental pH varies.[13–16] Examples of such organic molecules include fluorophores like fluorescein,[17] rhodamine,[18] Oregon Green 488,[19] and coumarin.[20] However, the accuracy of the pH measurement based on a single fluorescence emission intensity change is susceptible to both extrinsic and intrinsic factors, such as the stability of the excitation light, the concentration of the organic molecules, and finally the photobleaching of organic molecules. Therefore, efforts have been made to enhance the repeatability of fluorescent pH sensors using ratiometric detection, which can eliminate or alleviate the influence of environmental factors on the accuracy of the measurements.[21–24] These ratiometric sensors have fluorescence emissions with peaks of two different wavelengths and can be from different dyes or from the same dye that has two different emission wavelengths.

To achieve ratiometric measurements, one of the fluorescence emission peak intensities should be sensitive to the measurand, while the other emission peak intensity should be insensitive to the measurand and be used as the reference signal. By normalizing the measurand-sensitive peak intensity change with the measurand-insensitive peak intensity, the ratiometric measurements provide self-calibrated results with much better reliability. Specifically for pH sensing, the combination of the pH responsive dye and the reference dye should be carefully designed so that they can be excited by a single light source and the emission peak wavelengths are separated as far

Thayer School of Engineering, Dartmouth College, Hanover, 03755, NH, USA. E-mail: John.Zhang@Dartmouth.edu; Fax: +1 603 646 9024; +1 603 646 8787

† Electronic supplementary information (ESI) available. See DOI: https://doi.org/10.1039/d2na00943a

‡ These authors have contributed equally to this work.

apart from each other as possible to avoid signal distortions. Fluorescein isothiocyanate (FITC) is a commonly used indicator for pH monitoring and detection.[25,26] For example, Choudhary *et al.* explored the feasibility of coating fluorescein isothiocyanate (FITC) and tris(2,2′-bipyridyl)dichlororuthenium(II) hexahydrate ($Ru(BPY)_3$) onto nanoparticles as a ratiometric pH indicator-based sensor to study time-based or bacterial contamination associated milk degradation.[27]

Silica is an intrinsically non-toxic, environmentally friendly material possessing high mechanical strength. It is widely used in sensing applications due to the stable molecule encapsulating ability of its inorganic cage.[28] The use of silica-based materials for embedding and immobilizing pH-probes has been demonstrated.[29–31] In most studies, pH-probes are embedded in silica nanoparticles due to their unique properties like large specific surface area and thermal stability.[32,33] However, most of these nanosensors are used for imaging or intracellular pH monitoring. Immobilized pH sensors, rather than those that are floating, are more suitable for long-term *in situ* monitoring and avoid pollution from nanomaterials in wastewater.

In this work, a novel optical ratiometric pH sensing system based on dual-fluorescent hollow silica nanofibers (hSNFs) and an optical fiber detection system is demonstrated. To dope the FITC and $Ru(BPY)_3$ into the hSNFs, a straightforward doping method modified from previous work was adopted.[34–36] The developed doping procedure is integrated with the bottom-up synthesis procedure of the hSNFs, which allows the mass production of the nanofiber sensors. To the best of our knowledge, this is the first time that dual fluorophore doped hSNFs have been demonstrated, which addresses the limitation of long-term *in situ* pH metering using other nanoparticle-based pH sensors. The two doped fluorophores endow the hSNFs with a ratiometric pH sensing capability. Unlike a single molecule based optical sensor, dual fluorophore doped hSNFs are insensitive to photobleaching and environmental fluctuations. To enhance the *in situ* pH monitoring capability, the as-prepared fluorescent hSNFs can be deposited onto hydrophilic substrates, such as a plasma treated Petri dish (made of polystyrene). Using the customized optical fiber detection system (shown in Fig. 1), the sensitivity, reversibility, and stability of the dual fluorescent hSNFs' pH response were experimentally characterized. The developed pH sensors were tested within biological and environmental samples and showed pH measurements in accordance with a commercial pH meter. With the capability of local fluorescence detection, the hSNF-based optical pH sensing system is ideal for microscale sensing applications such as water quality monitoring and biological assays.

2 Experimental section

2.1 Materials and apparatus

Fluorescein isothiocyanate (FITC), tris(2,2′-bipyridyl)dichlororuthenium(II) hexahydrate ($Ru(BPY)_3$), 3-aminopropyl triethoxysilane (APTES), 1-pentanol, tetraethyl orthosilicate (TEOS),

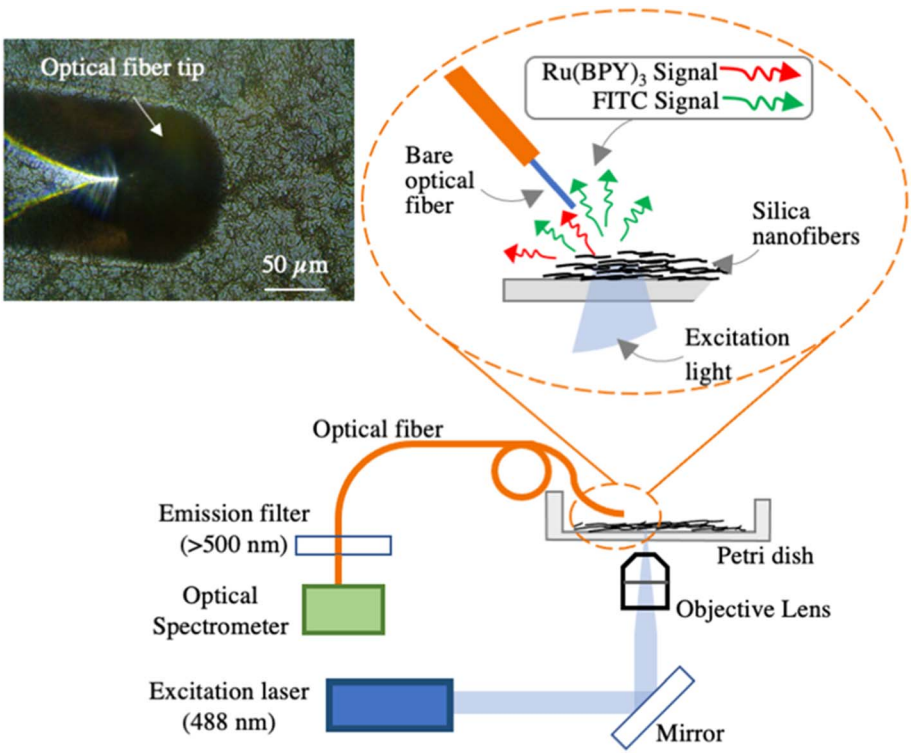

Fig. 1 Schematic of the dual fluorescent hSNF pH sensor and the optical characterization setup. The left upper inset is a microscope image of the tilted optical fiber tip positioned above the hSNFs.

trisodium citrate dihydrate, polyvinylpyrrolidone (PVP, 40 kDa), ammonium hydroxide (25 wt% aq.) and ethanol (200 proof) were purchased from Sigma-Aldrich. Colorless pH buffers were purchased from Sigma-Aldrich and Fisher Scientific. Polystyrene Petri dishes (Falcon 351008, 35 × 10 mm) were purchased from Corning Inc. The water used was from a Milli-Q ultrapure water purification system. All chemicals were used as received without any further purification.

A handheld high frequency generator (Electro-Technic Products, BD-20) was used for plasma treatment of the polymer surface. A portable pH meter (Apera Instruments, PH8500-MS) was used to measure pH values. Transmission electron microscopy (TEM) was performed on a Tecnai F20ST field emission gun (FEG) transmission electron microscope operating at an accelerating voltage of 200 kV. Scanning electron microscopy (SEM) was performed on a Thermo Scientific Helios 5CX Dual Beam scanning electron microscope. The energy-dispersive X-ray spectroscopy (EDS) measurements were performed with a spectrometer attached to the Tecnai F20ST FEG electron microscope. Fluorescence images were taken using an Olympus BX51 microscope.

2.2 Synthesis of hSNFs with internally doped $Ru(BPY)_3$

The $Ru(BPY)_3$ doped hSNFs were prepared following a reported method with modifications.[34,35] In a typical reaction, 5 mL of 1-pentanal and 0.5 g of PVP were first added to a 15 mL glass scintillation vial and mixed at 50 °C for 30 minutes. Then, 475 μL of ethanol, 100 μL of DI water and 40 μL of $Ru(BPY)_3$ solution (30 mM in water) were added to the mixed solution, and the mixture was vortexed for 1 min. Next, 50 μL of 0.18 M aqueous trisodium citrate dihydrate was injected and vortexed for 1 min, followed by the addition of 100 μL of ammonia hydroxide (25 wt% aq.) with vortex mixing for 1 min. Lastly, 50 μL of TEOS was injected and then immediately vortexed for 20 s. The mixtures reacted without stirring at 70 °C overnight for 12 h. After the reaction, the solution was poured into a 15 mL centrifuge tube, and 1 mL of acetone was added to break the microemulsion. hSNFs were isolated by centrifuging (1500 rpm, 15 min), and washed with water and ethanol (1000 rpm, 5 min) 3 times (ultrasonic cleaning, 5 min each time) to remove any surface impurities.

2.3 FITC coating on the surfaces of hSNFs

FITC was coated on the surfaces of hSNFs using a fluorescence coating method.[36] 20 mg of $Ru(BPY)_3$ doped hSNFs fabricated in the last step was dispersed in 2 mL ethanol in a 15 mL centrifuge tube. Next, 100 μL of ammonia hydroxide (25 wt% aq.), 100 μL of DI water and 20 μL of TEOS were added sequentially and vortexed for 20 s. 10 μL of FITC solution (15 mg FITC and 150 μL APTES reacted for 24 h in 1 mL of ethanol at room temperature) was then added. The above mixture was left without stirring at 40 °C for 8 h. The hSNFs doped with both FITC and $Ru(BPY)_3$ were isolated by centrifuging (700 rpm, 15 min), and washed 2 times with DI water (ultrasonic cleaning, 5 min each time) and 2 times with ethanol (ultrasonic cleaning, 5 min each time).

The length and diameter measurements of hSNFs were made in SEM images using the Line tool in ImageJ (50 total measurements). The shell thickness measurements of hSNFs were made in TEM images using the Line tool in ImageJ (25 total measurements).

2.4 Deposition of the dual fluorophore doped hSNFs

20 mg of the fabricated dual fluorescent hSNFs was dispersed in 1 mL ethanol. Petri dishes (Ø35 × H15 mm, polystyrene) were first plasma treated using a handheld high frequency generator for 1 min to induce a hydrophilic bottom surface by adding hydroxyl groups into hydrocarbon chains.[37] Right after the plasma treatment, 50 μL of the dual fluorescent hSNF solution was placed onto the center of a Petri dish, followed by the spin-coating process (200 rpm for 5 s, and 400 rpm for 15 s).

2.5 pH sensing based on the optical fiber readout system

To easily read out the fluorescence spectrum of the hSNFs, a customized fluorescence detection system based on optical fibers was developed, as shown in Fig. 1. The system consists of a 488 nm excitation laser (Techhood), an inverted microscope with a 20× objective lens (inverted metallurgical microscope, AmScope), a multimode optical fiber with a 105 μm diameter core (FG105UCA, Thorlabs), a 500 nm cut-on emission filter (FEL0500, Thorlabs), and an optical spectrometer (Flame Spectrometer, OceanOptics). The 488 nm laser was coupled to the inverted microscope and focused onto the sample by the 20× objective lens, which focussed the excitation light for the FITC and $Ru(BPY)_3$ fluorophores. The multimode fiber had a cleaved flat end and was pre-aligned to less than 3 μm above the silica nanofibers, as shown in the microscope image inset in Fig. 1. The optical fiber was tilted by a ~45° angle with respect to the plane of the hSNF coating to reduce the background light signal due to the transmitted excitation light. The emitted fluorescent light together with the scattered excitation light was collected by the multimode fiber and transmitted to an emission filter. The emission filter blocked light lower than 500 nm, which includes the 488 nm light from the excitation laser. This prevented the spectrometer from being overloaded by the strong scattered excitation light and the distortion of the fluorescence spectrum. Compared to fluorescent pH sensors based on microscope imaging,[11,29] in which the fluorescence signal is read out in the form of pixel intensities, the fiber-based system can read out the whole spectrum of the fluorescent signal in real-time. As will be detailed in Section 3.3, real-time pH measurements are based on this acquired fluorescence spectrum.

2.6 Preparation of real sample solutions

Tap water samples were collected at Thayer School of Engineering at Dartmouth (Hanover, New Hampshire, United States). Meltwater samples were collected after a winter storm (December 17th, 2022, Hanover, New Hampshire, United States) and melted at room temperature.

Commercially available human iPSC-derived cardiomyocytes (iCell2 cardiomyocytes, 01434) were obtained from Cellular

Dynamics International Inc. (CDI, Madison, WI, USA). Cryopreserved iCell2 cardiomyocytes were rapidly thawed, then diluted in iCell2 plating medium and seeded on 10% gelatin methacrylate hydrogel scaffolds fixed in no. 0 coverslip glass-bottom 12-well plates (MatTek). After 4 hours of post seeding, the plating medium was changed to a maintenance medium which was then changed every 48 hours. Cell cultures were maintained in an incubator at 37 °C having 5% CO_2 and 86% humidity. To make the gelatin methacrylate hydrogel scaffolds, type A porcine skin gelatin (3 g) was mixed at 10% (w/v) into Dulbecco's phosphate buffered saline (Gibco) at 60 °C and stirred until fully dissolved. Methacrylic anhydride (3 mL) was slowly added dropwise with stirring for 2 hours. After centrifugation to remove excess methacrylic acid, the supernatant was diluted at 2× volume, and dialyzed with 12 kDa MWCO tubing at 40 °C against distilled water for 7 days in a hood, with the buffer being changed twice daily. The pH of the resulting gelatin methacryloyl (GelMA) solution was neutralized to 7.4 using 1 M $NaHCO_3$, and filter-sterilized with a rapid vacuum PES membrane filter unit. The sterile GelMA solution underwent rapid freezing at −80 °C for 1 hour, and was then lyophilized at −80 °C for 72 hours to form a white porous foam which was stored at −20 °C until use.

3 Results and discussion

3.1 Synthesis of the dual fluorescent hSNFs

The synthesis of the dual fluorescent hSNFs is illustrated in Fig. 2. The design is based on the consideration that the fluorophore $Ru(BPY)_3$ is doped into the hSNFs during TEOS hydrolysis as a reference dye, while fluorophore FITC is coated on the surfaces of the hSNFs enabling pH response. Due to the solution–liquid–solid (SLS) mechanism, a microemulsion system is created by dispersing the catalyst liquid phase (water droplets) into the solution phase (pentanol); then, the precursor (TEOS) diffuses from the solution phase into the liquid phase to form target monomers (silica oligomers).[38] In these experiments, hydrolyzed TEOS molecules (silica oligomers) were formed on the droplet surface at high ammonia content and were deposited immediately as solid silica before reaching the droplet center,[39] so that hSNFs were synthesized instead of solid silica nanorods. The synthesis process can be summarized as follows: firstly, $Ru(BPY)_3$ was dissolved in the water droplets in the microemulsion and encapsulated inside the hollow center of the hSNFs. Then, the FITC–APTES conjugate was grafted onto a silica matrix while additional TEOS was added to grow a thin silica film simultaneously.[40] The hollow structure allowed most of the $Ru(BPY)_3$ to locate inside the SNFs, which prevented

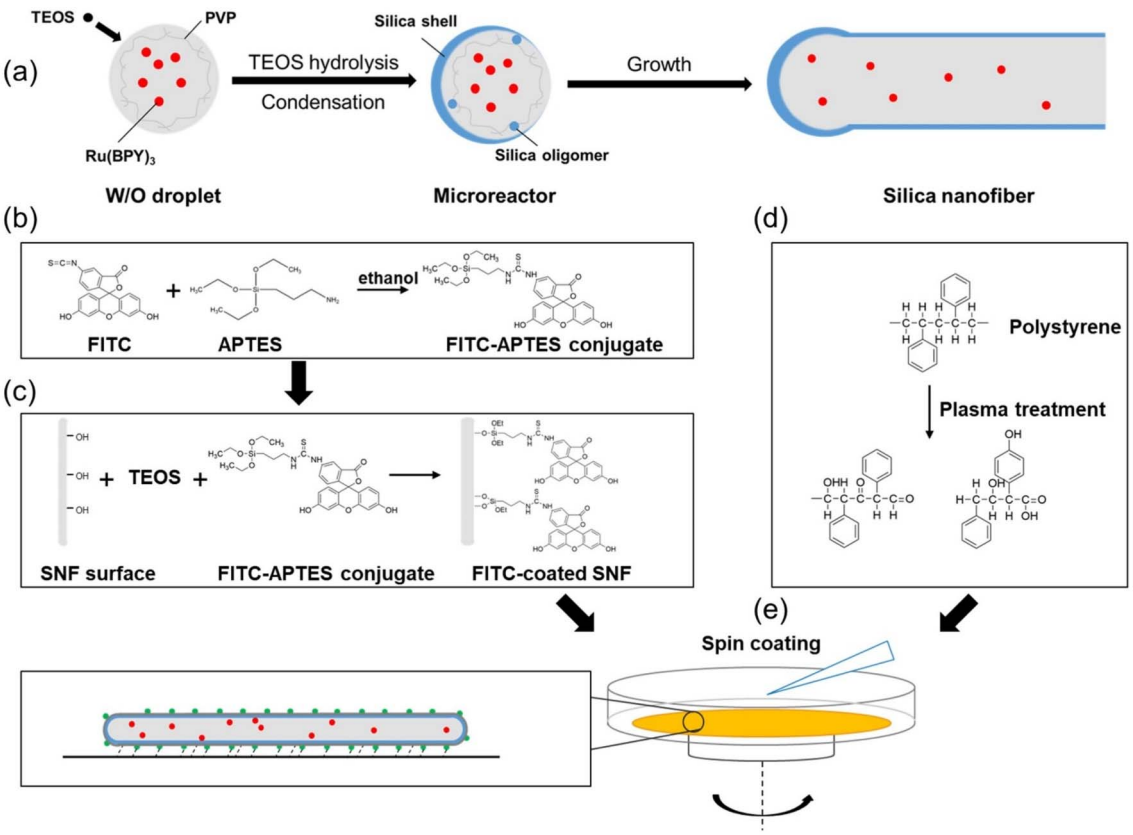

Fig. 2 Schematics of the hSNF synthesis, surface coating and deposition process. (a) Synthesis of an hSNF containing $Ru(BPY)_3$ in the water-in-oil microemulsion. (b) Reaction of FITC and APTES to form a conjugate molecule. (c) Coating process of the FITC–APTES conjugate on the surface of an SNF. (d) Plasma treatment of the polystyrene material. (e) Deposition of the dual fluorescent hSNFs onto the plasma treated Petri dish.

interaction with the environment and made it a stable reference signal in the ratiometric measurement. Coating FITC outside allowed it to respond to environmental pH variations.

3.2 Morphological and optical properties of the silica nanofibers

The average length of hSNFs before coating FITC is (6.20 ± 1.59) μm and the average diameter is (238 ± 51) nm. By adjusting the reaction parameters (*i.e.*, concentration of chemical reagents, temperature, and reaction time), a relatively long aspect ratio of 26.5 is obtained. The shell thickness of hSNFs is about 41 nm (Fig. 3). After coating with FITC, the average diameter of hSNFs is increased to around 410 nm.

Energy-dispersive X-ray spectroscopy (EDS) was used to characterize the elements of the dual fluorescent hSNFs. As shown in Fig. 4, the presence of elements silicon (Si), carbon (C), oxygen (O), sulfur (S), and ruthenium (Ru) is confirmed from the EDS spectrum. The element silicon is from the hSNFs. The element sulfur exists only in FITC molecules while the element ruthenium is only from $Ru(BPY)_3$ molecules.

To further confirm that FITC and $Ru(BPY)_3$ fluorophores have been successfully doped into the hSNFs and to identify the fluorescence peak wavelengths of the dual fluorescent hSNFs, analysis of four emission spectra was performed using a microplate reader (BioTek). Fig. 5a and b compare the emission spectra of FITC and $Ru(BPY)_3$ fluorophores directly dissolved in water and that of hSNFs doped with only FITC or $Ru(BPY)_3$. These comparisons confirm that FITC and $Ru(BPY)_3$ fluorophores have been successfully doped into the hSNFs. It is noted that the fluorescence peak wavelengths of both FITC and $Ru(BPY)_3$ have shifted after being coated onto the SNFs. These shifts are due to the coupling of the transition dipole moment of the fluorophores with the silica nanofibers and the change of the fluorophores' molecular conformation.[41] The emission spectrum of the dual fluorescent hSNFs was used to identify the fluorescence peaks of FITC and $Ru(BPY)_3$, as shown in Fig. 5c. The results show that the FITC and $Ru(BPY)_3$ peaks of the dual fluorescent hSNFs are at around 515 nm and 595 nm, respectively. These peak wavelengths are used in the following pH sensing experiments to calculate the FITC and $Ru(BPY)_3$ intensity ratio ($I_{FITC}/I_{Ru(BPY)_3}$ ratio).

3.3 pH sensing of the dual fluorescent hSNF coated substrate

The pH responses of the dual fluorescent hSNFs were experimentally characterized using the optical characterization setup shown in Fig. 1. In the experiments, the environmental pH of the dual fluorescent hSNF coated Petri dish was changed from alkaline (pH = 9.0) to acidic (pH = 4.0) by replacing colorless pH buffer solutions. The fluorescence spectra of the dual

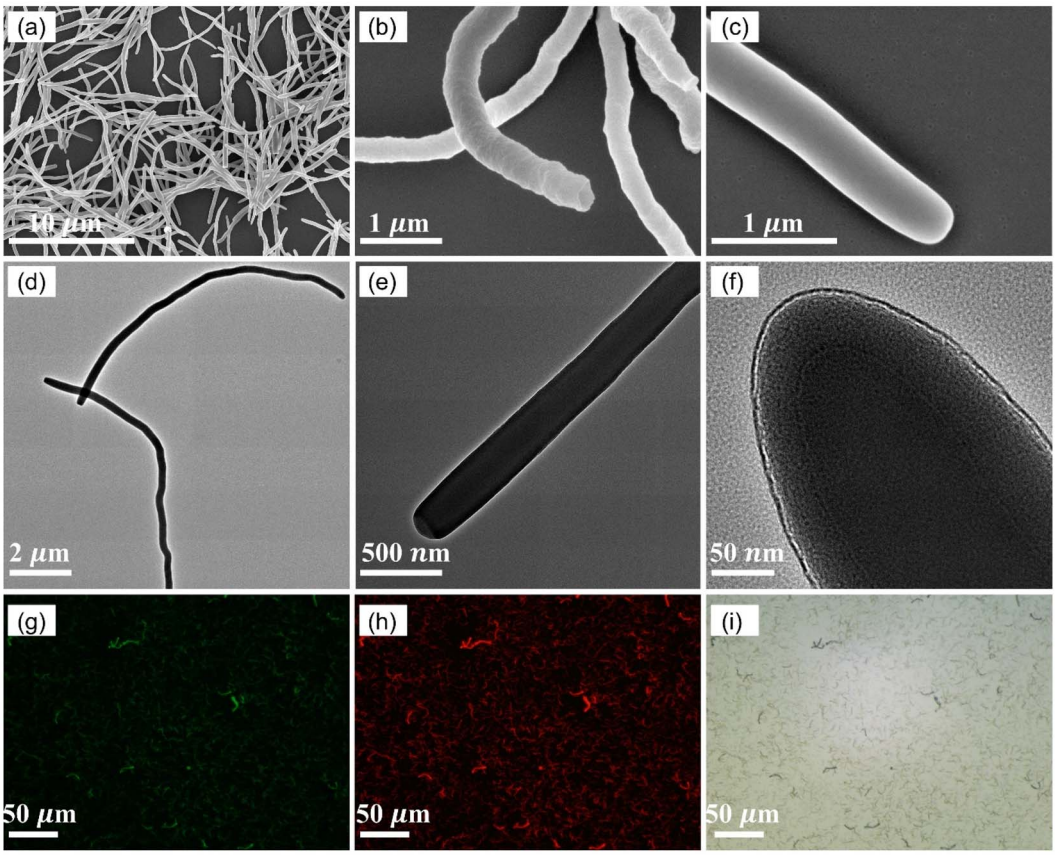

Fig. 3 Characterization of hSNFs. (a–c) SEM images of hSNFs. hSNFs (b) before and (c) after FITC coating. (d–f) TEM images of hSNFs at different scales. (g and h) Fluorescence images of FITC and $Ru(BPY)_3$. (i) Bright field images of hSNFs on the polystyrene substrate.

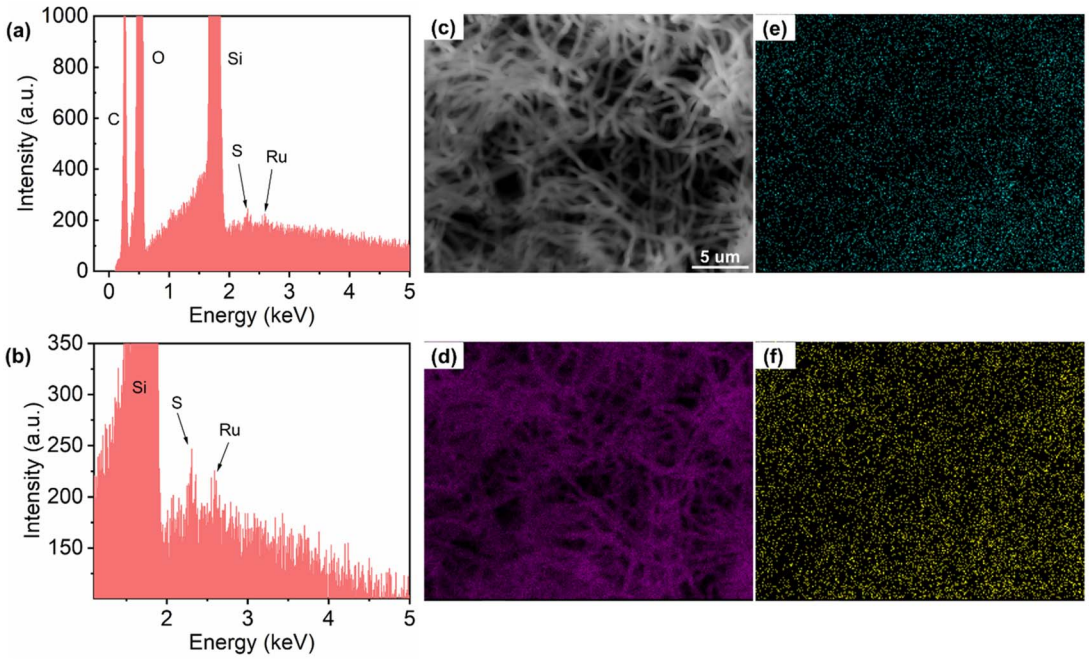

Fig. 4 EDS characterization of dual fluorescent hSNFs. (a) The EDS energy spectrum of dual fluorescent hSNFs and (b) its enlarged view showing the peaks of elements S and Ru. (c) Field of view of the EDS map. EDS elemental mapping of (d) Si, (e) S and (f) Ru.

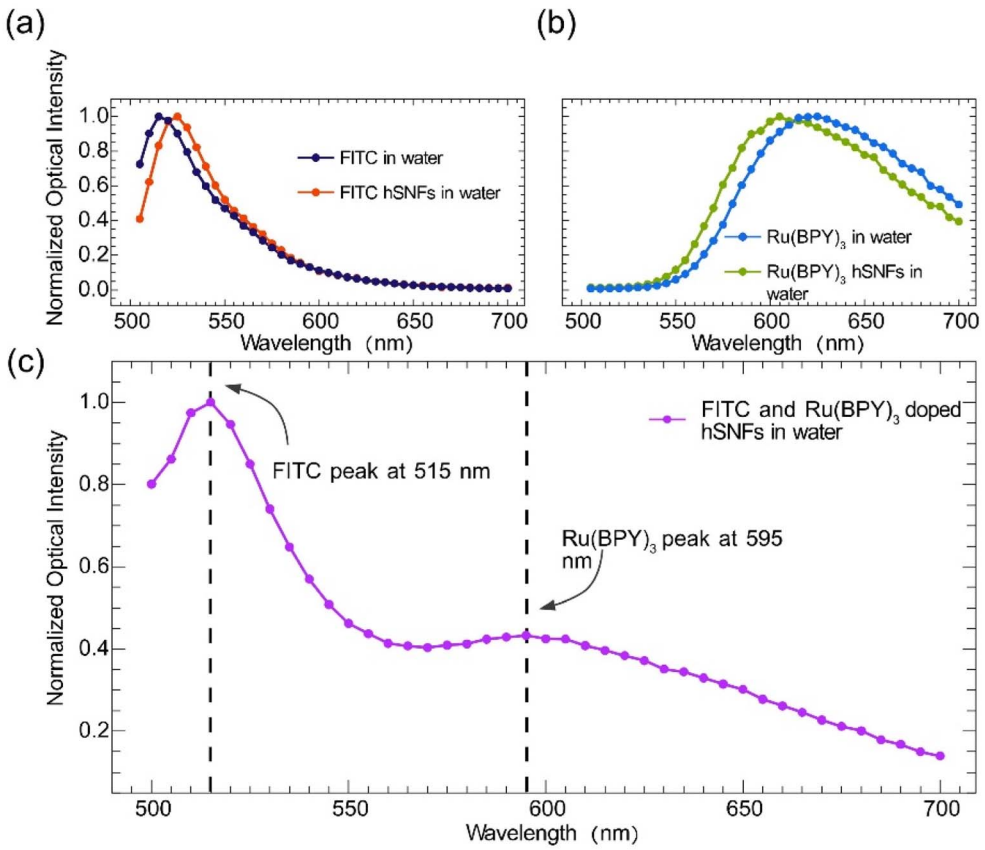

Fig. 5 Emission spectra of fluorophores and the dual fluorescent hSNFs. (a) Emission spectra of FITC dissolved in water and FITC coated hSNFs dissolved in water. (b) Emission spectra of $Ru(BPY)_3$ dissolved in water and $Ru(BPY)_3$ coated hSNFs dissolved in water. (c) Emission spectrum of hSNFs coated with both FITC and $Ru(BPY)_3$.

fluorescent hSNFs at six different pH values were characterized (Fig. S1†). At each pH value, spectra were recorded with an exposure time of 1 s. The fluorescence signals collected by the optical fiber may vary in intensity due to some factors such as distance between the optical fiber and hSNFs. To confirm that the fluorescence intensity change does not affect the pH measurement, we place the optical fiber at three different places with the same angle and collect the spectra in colorless pH 7.0 buffer (Fig. 6a and b). The inserted figure in Fig. 6a indicates the ratio of FITC to $Ru(BPY)_3$ intensity. The results show that despite the intensity change, the intensity ratios of the three conditions are almost the same, with a relative standard deviation (RSD) of 9%. The ratiometric characterization method proves the stability of the dual fluorescent hSNFs for pH measurement. Fig. 6c shows the calculated $I_{FITC}/I_{Ru(BPY)_3}$ ratio plotted against the pH values. A linear regression model is used to characterize the relationship between the $I_{FITC}/I_{Ru(BPY)_3}$ ratio and the pH values. The fitting results show that the $I_{FITC}/I_{Ru(BPY)_3}$ ratio has a linear relationship with the pH value and a pH sensitivity of 0.248 [pH^{-1}]. The strength of the linear fitting is characterized using the coefficient of determination (R^2 value), which is calculated to be 0.986.

We also find that the dual fluorescent hSNFs show excellent reversibility in monitoring pH. Fig. 6d and e show the optical spectra collected in the experiment where the pH of the solution was changed periodically between pH 5.0 and pH 8.0 buffer. The $I_{FITC}/I_{Ru(BPY)_3}$ ratio at each cycle is plotted in Fig. 6f. It is evident that the ratio can be completely recovered when the solution is replaced between the buffers with pH 5.0 and pH 8.0. These results indicate that the synthesized dual fluorescent hSNFs are

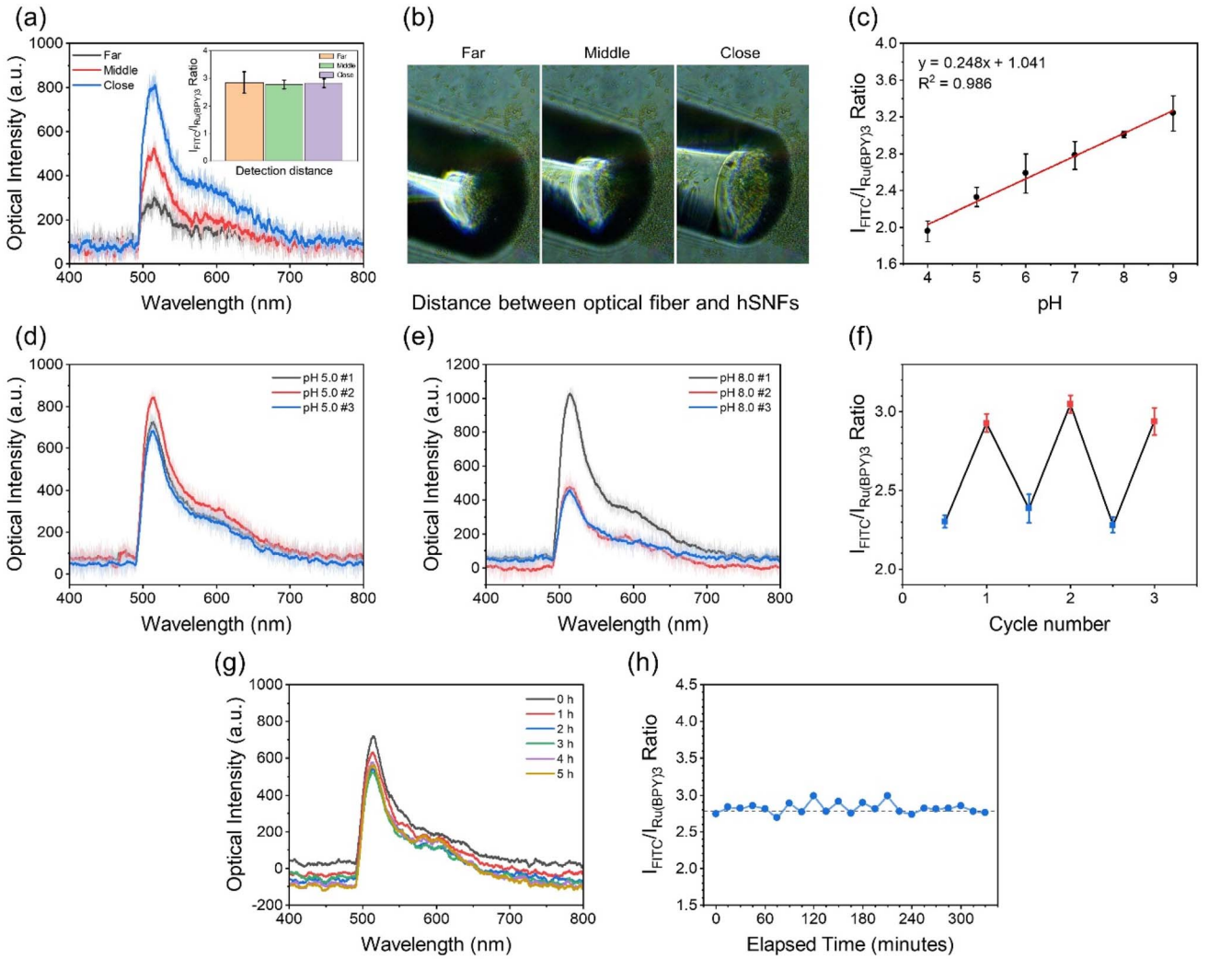

Fig. 6 Characterization of the pH response of the dual fluorescent hSNFs. (a) The optical spectra of the dual fluorescent hSNFs collected at different locations with error bars (the shaded area). The inserted figure indicates the $I_{FITC}/I_{Ru(BPY)_3}$ ratio at each location. (b) Optical images of the optical fiber collecting signals at different distances. (c) Linear fitting of the $I_{FITC}/I_{Ru(BPY)_3}$ ratio against different pH values. (d) The optical spectra of the dual fluorescent hSNFs measured in pH 5.0 buffer solution in different cycles. (e) The optical spectra of the dual fluorescent hSNFs measured in pH 8.0 buffer solution in different cycles. (f) The plot of the $I_{FITC}/I_{Ru(BPY)_3}$ ratio at different cycles calculated from the spectra in (d) and (e). (g) The optical spectra of the dual fluorescent hSNFs measured in the pH 7 buffer solution over 5 hours. (h) The plot of the $I_{FITC}/I_{Ru(BPY)_3}$ ratio at different elapsed times. The dashed line represents the value of the $I_{FITC}/I_{Ru(BPY)_3}$ ratio at pH 7.0 obtained from the linear fitting.

a reversible and robust ratiometric pH indicator. Additionally, the pH response of the sensor was found to be rapid (less than 10 s). It is expected to benefit from the large surface-to-volume ratio of hSNFs, which provides efficient contact of the pH sensitive dye (FITC) with the analyte within the aqueous medium.

The ratiometric characterization method based on the FITC and $Ru(BPY)_3$ fluorescence intensity ratio can effectively decouple the pH induced FITC fluorescence intensity variation from that caused by photobleaching. Such decoupling is particularly beneficial in long-term measurements, where the accumulated exposure time is often long enough to induce photobleaching of the fluorophores. Here, the effectiveness of the ratiometric characterization method in long-term pH sensing applications was experimentally demonstrated. In this experiment, a dual fluorescent hSNF coated Petri dish was filled with a buffer solution (pH 7.0). The fiber-based fluorescence detection system was used to read out the fluorescence spectra every 15 minutes for more than 5 hours. As shown by the recorded spectra in Fig. 6g, there are slight decreases in the fluorescence intensities for both FITC and $Ru(BPY)_3$, which is caused by the photobleaching. However, as shown in Fig. 6h, the $I_{FITC}/I_{Ru(BPY)_3}$ ratio calculated based on the optical spectra in the first 5 hours had no significant decrease and had only minimum fluctuations, which matched the fact that the buffer solution had a constant pH. These results show that the $I_{FITC}/I_{Ru(BPY)_3}$ ratio is not affected by the photobleaching of the fluorophores for at least 5 hours of periodic laser irradiation, and reliably represents the solution pH value. When stored under dark conditions, degradation of fluorescent moieties was not observed for up to one month (Fig. S2†).

3.4 Sensing study within environmental and biological samples

Owing to the excellent stability and good sensitivity of the dual fluorescent hSNFs for pH measurement within aqueous media, it is worth exploring the capability of this pH indicator within environmental and biological samples. To verify the pH monitoring performance of this ratiometric pH sensor, environmental samples (tap water and meltwater) and biological samples (cell culture media) were analyzed.

Water is essential for sustaining life, and clean water is critical to health and well-being. Water pH is one important factor concerning water quality. Herein, we collected water samples and measured the pH values using both a commercial pH meter and the dual fluorescent hSNF pH indicator. The detected results of pH in tap water and meltwater using this sensor are in accordance with those obtained from the conventional pH meter (Fig. 7a and b), with differences of 0.7% and 3.4%, respectively. The optical spectra are shown in Fig. S3.†

Human induced pluripotent stem cell-derived cardiomyocytes (hiPSC-CMs) were chosen as a biological sample for evaluating the pH measurement performance. hiPSC-CMs are widely used in studying cell energy metabolism.[42] Metabolism is a continuous source of acids, because the process of cellular activities (the tricarboxylic acid cycle and glycolysis) will produce H^+ in aqueous media.[43] Therefore, monitoring extracellular pH is a simple and powerful way to determine cell metabolic activities. In the experiment, 2 mL of the cell culture media was collected every 48 hours following the second day of culture. The optical spectra of the cell culture media are shown in Fig. S3,† and the calculated $I_{FITC}/I_{Ru(BPY)_3}$ ratios are plotted in Fig. 7c. The pH value of the cell culture media noticeably decreases from around pH 7.5 to pH 7.3, suggesting increased cell metabolic activities of hiPSC-CMs over time. In the meantime, the cardiomyocytes beating frequency in culture media decreases from around 30 beats per min during Day 2 to 24 beats per min at Day 4 and 21 beats per min at Day 6 (shown in Movies S1–S3†). The minimal sample size has also been determined to be 50 μL to ensure that the optical fiber tip is immersed in the sample solution (Fig. S4†).

In this work, we designed and synthesized a pH sensor integrating two fluorophores (FITC and $Ru(BPY)_3$) into hollow silica nanofibers. The comprehensive spectroscopic characterization illustrated that this new fluorescent indicator can be used for monitoring pH in a ratiometric method from two separate wavelengths, *i.e.* 515 and 595 nm, with one excitation light source. Table S1† shows a comparison of some key parameters that are used to evaluate the fluorescent pH sensor

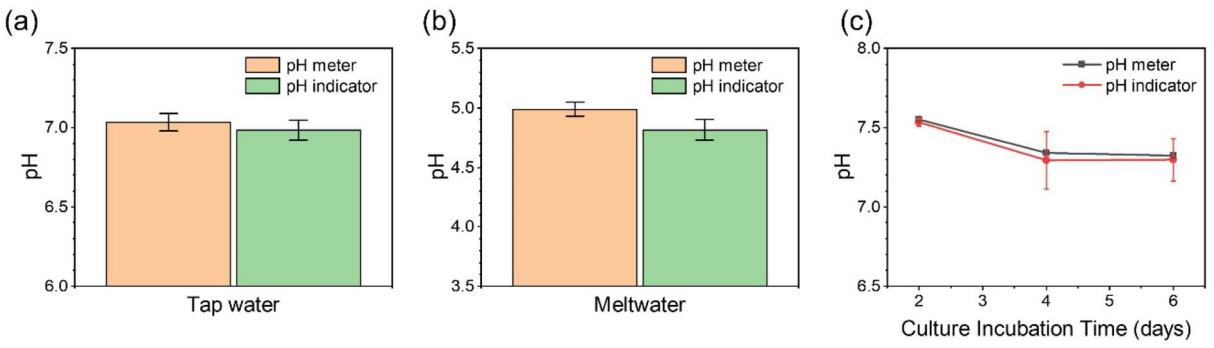

Fig. 7 Real sample assay. The pH measurement results of tap water (a), meltwater (b) and hiPSC-CMs cell culture media (c) samples from the commercial pH meter and dual fluorescent hSNF pH sensor.

including the detection device, system configuration, portability, number of excitation light sources, pH range, linearity, reversibility, and immobilization of nanoparticles for some prominent fluorescent pH sensors developed since 2013. The dual fluorescent hSNFs developed in this work have comprehensively strong performances in all aspects listed in this table. Unlike other pH probes that are read out using a large microscope or fluorometer, this pH sensor uses a tiny fiber-optic spectrometer as the detector with high portability. The dual fluorescent hSNFs are excited by a single excitation light source at 488 nm and exhibit superb linearity in a large pH range (pH 4.0–9.0). The immobilization strategy of coating the pH sensor onto the plasma treated polystyrene substrate facilitates excellent reversibility and minimizes sample volume requirement, as well as avoiding pollution from nanomaterials in wastewater.

4 Conclusions

In summary, a novel ratiometric fluorescent pH sensor based on hSNFs doped with FITC and $Ru(BPY)_3$ fluorophores was developed. Using water-in-oil droplets created in a microemulsion system, dual fluorophore doped hSNFs with emission peaks at around 515 nm and 595 nm were synthesized in a straightforward fashion. The pH response of the dual fluorescent hSNFs was characterized using a customized optical fiber-based fluorescence detection system. The characterization results show that the dual fluorescent hSNFs have a pH sensitivity of 0.248 [pH^{-1}] and a response time of less than 10 s. Thanks to the ratiometric measurement approach based on the FITC and $Ru(BPY)_3$ fluorescence intensity ratio, the developed fluorescent pH sensor can achieve long term pH measurements with only minimum influence from photobleaching. It is experimentally demonstrated that the sensor has a linear pH response within the pH 4.0–9.0 range and long-term stability for more than 5 hours. The sensor shows great accuracy in pH measurement compared to a traditional pH meter. Owing to the immobilization on a Petri dish, the sensor requires much less sample volume (50 μL), making it suitable for assaying microscopic biological samples. Beyond the demonstrated pH sensing application, the developed rational synthesis method of hSNFs paves the way towards enabling a broad class of sensing applications with the fluorophore-doped devices.

Conflicts of interest

The authors declare that they have no known competing financial interests or personal relationships that could have appeared to influence the work reported in this paper.

Acknowledgements

The authors would like to acknowledge financial support from the Agilent University Research Program [grant number 1509369]. We gratefully acknowledge the support from the Electron Microscope Facility at Dartmouth College.

References

1 H. C. Boyer, K. Gorkowski and R. C. Sullivan, *Anal. Chem.*, 2020, **92**, 1089–1096.
2 Y. Zhou, L. A. Mur, A. Edwards, J. Davies, J. Han, H. Qin and Y. Ye, *Water Sci. Technol.*, 2018, **78**, 432–440.
3 A. Kurkdjian and J. Guern, *Annu. Rev. Plant Physiol. Plant Mol. Biol.*, 1989, **40**, 271–303.
4 X. Liu, Y. Su, H. Tian, L. Yang, H. Zhang, X. Song and J. W. Foley, *Anal. Chem.*, 2017, **89**, 7038–7045.
5 M. Hu, W. Zhao, H. Li, J. Gu, Q. Yan, X. Zhou, Z. Pan, G. Cui and X. Jiao, *BMC Vet. Res.*, 2018, **14**, 1–8.
6 V. Khramtsov, *Curr. Org. Chem.*, 2005, **9**, 909–923.
7 O. Kreft, A. M. Javier, G. B. Sukhorukov and W. J. Parak, *J. Mater. Chem.*, 2007, **17**, 4471–4476.
8 H. Kaden, H. Jahn and M. Berthold, *Solid State Ionics*, 2004, **169**, 129–133.
9 S. Lee, W. Cho and J. Lee, *Korean J. Chem. Eng.*, 2013, **30**, 1008–1012.
10 S. Bargrizan, R. J. Smernik and L. M. Mosley, *Soil Sci. Soc. Am. J.*, 2017, **81**, 1350–1358.
11 J. Shangguan, D. He, X. He, K. Wang, F. Xu, J. Liu, J. Tang, X. Yang and J. Huang, *Anal. Chem.*, 2016, **88**, 7837–7843.
12 D. Aigner, B. Ungerböck, T. Mayr, R. Saf, I. Klimant and S. M. Borisov, *J. Mater. Chem. C*, 2013, **1**, 5685–5693.
13 L. Yang, Y. Ren, W. Pan, Z. Yu, L. Tong, N. Li and B. Tang, *Anal. Chem.*, 2016, **88**, 11886–11891.
14 G. Sevinç, B. Küçüköz, H. Yılmaz, G. Şirikçi, H. G. Yaglioglu, M. Hayvalı and A. Elmali, *Sens. Actuators, B*, 2014, **193**, 737–744.
15 S. L. Shen, X. P. Chen, X. F. Zhang, J. Y. Miao and B. X. Zhao, *J. Mater. Chem. B*, 2015, **3**, 919–925.
16 X. Yuan, T. Zhang, J. Yan, X. Chen, L. Wang, X. Liu, K. Zheng and N. Zhang, *Dyes Pigm.*, 2020, **177**, 108318.
17 G. Li, B. Zhang, X. Song, Y. Xia, H. Yu, X. Zhang, Y. Xiao and Y. Song, *Sens. Actuators, B*, 2017, **253**, 58–68.
18 S. G. Stratton, G. H. Taumoefolau, G. E. Purnell, M. Rasooly, W. L. Czaplyski and E. J. Harbron, *Chem. – Eur. J.*, 2017, **23**, 14064–14072.
19 M. Schwamborn, J. Schumacher, J. Sibold, N. K. Teiwes and C. Steinem, *Analyst*, 2017, **142**, 2670–2677.
20 J. Joniak, H. Stankovičová, J. Filo, K. Gaplovská-Kyselá, V. Garaj and M. Cigáň, *Sens. Actuators, B*, 2020, **307**, 127646.
21 Q. Chen, X. Liu, J. Chen, J. Zeng, Z. Cheng and Z. Liu, *Adv. Mater.*, 2015, **27**, 6820–6827.
22 Y. H. Chan, C. Wu, F. Ye, Y. Jin, P. B. Smith and D. T. Chiu, *Anal. Chem.*, 2011, **83**, 1448–1455.
23 Y. Chen, C. Zhu, J. Cen, Y. Bai, W. He and Z. Guo, *Chem. Sci.*, 2015, **6**, 3187–3194.
24 W. Song, W. Duan, Y. Liu, Z. Ye, Y. Chen, H. Chen, S. Qi, J. Wu, D. Liu, L. Xiao, C. Ren and X. Chen, *Anal. Chem.*, 2017, **89**, 13626–13633.
25 R. Gui, X. An and W. Huang, *Anal. Chim. Acta*, 2013, **767**, 134–140.
26 X. Zhu, H. Jin, C. Gao, R. Gui and Z. Wang, *Talanta*, 2017, **162**, 65–71.

27 S. Choudhary, B. Joshi, G. Pandey and A. Joshi, *Sens. Actuators, B*, 2019, **298**, 126925.
28 S. Islam, H. Bakhtiar, W. N. W. Shukri, M. S. abd Aziz, S. Riaz and S. Naseem, *Microporous Mesoporous Mater.*, 2019, **274**, 183–189.
29 S. Fulaz, D. Hiebner, C. H. N. Barros, H. Devlin, S. Vitale, L. Quinn and E. Casey, *ACS Appl. Mater. Interfaces*, 2019, **11**, 32679–32688.
30 Y. Toum Terrones, F. Coluccio Leskow, A. V. Bordoni, S. L. Acebedo, C. C. Spagnuolo and A. Wolosiuk, *J. Mater. Chem. B*, 2017, **5**, 4031–4034.
31 L. Dai, Q. Zhang, J. Li, X. Shen, C. Mu and K. Cai, *ACS Appl. Mater. Interfaces*, 2015, **7**, 7357–7372.
32 Q. L. Li, S. H. Xu, H. Zhou, X. Wang, B. Dong, H. Gao, J. Tang and Y. W. Yang, *ACS Appl. Mater. Interfaces*, 2015, **7**, 28656–28664.
33 W. Cheng, J. Nie, L. Xu, C. Liang, Y. Peng, G. Liu, T. Wang, L. Mei, L. Huang and X. Zeng, *ACS Appl. Mater. Interfaces*, 2017, **9**, 18462–18473.
34 M. Araghi, M. Ghahari and M. Shafiee Afarani, *J. Environ. Chem. Eng.*, 2017, **5**, 1780–1790.
35 R. P. Murphy, K. Hong and N. J. Wagner, *J. Colloid Interface Sci.*, 2017, **501**, 45–53.
36 H. Ma, P. Gong, Y. Qiao, Y. Huang, C. B. Park, H. Jiang and G. Li, *Prog. Org. Coat.*, 2021, **154**, 106183.
37 A. Suganya, G. Shanmugvelayutham and J. Hidalgo-Carrillo, *Plasma Chem. Plasma Process.*, 2018, **38**, 1151–1168.
38 A.-Q. Zhang, H.-J. Li, D.-J. Qian and M. Chen, *Nanotechnology*, 2014, **25**, 135608.
39 J. Dou, Y. Sheng, C. Choong, L. Chen and H. C. Zeng, *Appl. Catal., B*, 2017, **219**, 580–591.
40 A. Kuijk, A. Van Blaaderen and A. Imhof, *J. Am. Chem. Soc.*, 2011, **133**, 2346–2349.
41 J. Kerfoot, V. V. Korolkov, A. S. Nizovtsev, R. Jones, T. Taniguchi, K. Watanabe, I. Lesanovsky, B. Olmos, N. A. Besley, E. Besley and P. H. Beton, *J. Chem. Phys.*, 2018, **149**, 054701.
42 B. M. Ulmer and T. Eschenhagen, *Biochim. Biophys. Acta, Mol. Cell Res.*, 2020, **1867**, 118471.
43 S. A. Mookerjee, R. L. S. Goncalves, A. A. Gerencser, D. G. Nicholls and M. D. Brand, *Biochim. Biophys. Acta, Bioenerg.*, 2015, **1847**, 171–181.